EFFECTIVE VENTILATION

9th AIVC Conference, Gent, Belgium
12-15 September, 1988

Paper 6

VENTILATION GENERATED BY A FLUCTUATING PRESSURE DIFFERENTIAL

B SAHIN [1], C CLARK [2], A J REYNOLDS [1], R WAKELIN [1]

Brunel University
Kingston Lane
Uxbridge, Middlesex
UB8 3PH, England

1 - Department of Mechanical Engineering
2 - Department of Manufacturing and Engineering Systems

1. SYNOPSIS

Ventilation produced by fluctuating pressure differences across a building appears to have received little attention. Such fluctuations are produced by gustiness of the wind or turbulence in the flow around a building.

An experimantal study has been performed on a laboratory model to investigate unsteady flows through apertures simulating those in the fabric of a building. Independent variables investigated were the mean pressure difference ($\bar{p}$) across the aperture and the amplitude (p_o) and frequency (f) of a superimposed fluctuating pressure difference to give $p(t) = \bar{p} + p_o \sin 2\pi f t$. The relative amplitude ($p_o/\bar{p}$) range covered was 0.2 to 0.97 and the frequency range was 0.02 to 0.6 Hz. A number of aperture geometries has been investigated.

Measurements were made of instantaneous pressure difference across the aperture, air flow rate into the plenum chamber supplying the aperture and velocity of air issuing from the aperture. The relationship between pressure difference and flow was characterised by a discharge coefficient, (Cd). Cd values based upon the instantaneous measurements were plotted throughout a flow cycle for each operating condition. This produced a Cd loop, the size of which depended upon $p_o/\bar{p}$ and the Strouhal number. Time-averaged flows were characterised by two Cd values, based upon root mean pressure difference and the mean pressure difference, respectively. Measured values of Cd were compared with the results of a theoretical analysis which predicted successfully the general features observed.

2 LIST OF SYMBOLS

A - cross-sectional area (m^2)

C_c - coefficient of contraction

C_d - discharge coefficient

C_{ds} - discharge coefficient for steady flow

C_f - skin-friction coefficient

D - diameter of circular cross-section aperture (m)

f - fluctuation frequency (Hz), = $\omega/2\pi$.

k - friction factor

ℓ - distance from vena-contracta to end of aperture (m)

L - length of aperture (m)

$\mathcal{L}$ - inertial equivalent length (m), see equation 2.

m - mass (kg)

p - pressure (Pa)

p_m - mean pressure (Pa)

p_o - amplitude of fluctuating component of pressure (Pa)

r - space coordinate in radial direction

R - relative flow rate amplitude (= $\dot{V}_o/\bar{\dot{V}}$)

R_g - characteristic gas constant (kJ/kg K)

R_p - relative pressure amplitude (= P_o/Pm)

St - Strouhal number ($St = fD/v = \omega D^3/8\bar{\dot{V}}$)

St^* - modified Strouhal number (= $St\,\mathcal{L}/D$)

t - time (s)

T - absolute temperature (K)

v - velocity (m/s)

$\dot{V}$ - volume flow rate (m^3/s)

$\bar{\dot{V}}$ - mean volume flow rate (m^3/s)

$\dot{V}_o$ - amplitude of fluctuating component of flow rate (m^3/s)

z - space coordinate in axial direction

α, β - non-uniformity coefficients, see equation 8.

γ - ratio of gas specific heats

ρ - density (kg/m^3)

τ_o - skin-friction (N/m^2)

ω - radian frequency (s^{-1})

3. INTRODUCTION

An aspect of building ventilation which is still not well understood is the effects of fluctuations in the external pressure. These fluctuations arise from gustiness of the wind approaching a building and unsteadiness in the separated flows around it.

The effective ventilation rate through an aperture will depend upon its geometry and upon the frequency of pressure fluctuations and on the ratio of their amplitude to the mean differential across the aperture. The relationship between a fluctuating pressure differential and flow through a plane aperture has been investigated by Earles and Zarek (1963), Karim and Rashidi (1972), and Mohammad and Mottram (1981), in relation to pulsating flow measurement with an orifice-meter. Because this relationship is non-linear, published work has concentrated mainly on the correction factors required to allow a correct mean flow rate to be inferred from a measured fluctuating pressure differential.

The broad objective of the present work was to look at the pressure difference/flow realtionship in more detail, both experimentally and theoretically. To date, investigations have been restricted to regular pressure pulsations of simple-harmonic form but without flow reversal.

4. EXPERIMENTAL STUDY

4.1 Test-rig and instrumentation

Experimental studies were carried out using the purpose built rig shown in Fig. 1 into which a variety of aperture geometries representative of those occurring in buildings can readily be introduced. This apparatus provides for the superimposition upon a mean differential of pressure, variations of the frequencies and amplitudes typical of those likely to arise in the field. It was designed to permit modifications to allow representation of (a) flow reversal during the cycle of pressure variation and (b) a cross-flow on one or both sides of the aperture.

The inset in Fig. 1 shows the method used to produce a periodic fluctuation in the pressure generated by a constant speed fan: a motor driven disc rotates at constant speed about a point (marked +) eccentric to the centre of a circular aperture

(marked •). By changing the speed of rotation and the degree of eccentricity a variety of fluctuations can be generated about a mean pressure differential between the plenum chamber and atmosphere.

Air passes into the plenum from a plastic tube of diameter 55mm which contains screens and a flow straightener to improve the quality of flow before flow measurement. This is achieved using a velocity transducer (TSI, model 1610-13) which was calibrated against a series of standard orifice meters which were introduced into the supply tube well upstream of the transducer. This provided a relationship between transducer signal and volume flow rate into the plenum chamber.

Pressure within the plenum is measured with a single-ended transducer (Gaeltec, model 3CT). Outflow from the aperture is to atmosphere, so the measured pressure is also the pressure differential across the aperture. The discharge coefficient for the aperture under test was calculated from instantaneous values of pressure difference, Δp, and flow, using:

$$C_d = \frac{\dot{V}}{A_o(2\Delta p/\rho)^{1/2}}$$

Velocity measurements were also made at the aperture outflow and velocity coefficients determined, but these results are not reported here. All data were digitised and stored in a microcomputer for subsequent processing.

4.2 Results

Results are presented for 3 aperture geometries all of circular cross-section, with diameter, D = 25mm. The first is a plane square-edged orifice; the other two are of cylindrical form with length L to give L/D = 1 and 10, respectively. Tests were carried out for inertia dominated flows with mean flow. Reynolds numbers in the range 7,000 to 24,000 and fluctuation frequencies form 0.02 to 0.6 Hz.

Figure 2 shows the values of the discharge coefficients under steady flow conditions, for the three aperture geometries, as functions of the volume flow through the aperture. The anticipated variations in C_d at low Reynolds numbers, are shown in Fig 2 and these are succeeded by generally more uniform values at higher Reynolds numbers. Note that the reattachment and pressure recovery achieved in the short tube (L/D = 1) increase the flow achieved for a particular

pressure differential by some 25 per cent, in comparison with the flow through a simple orifice. The outflow through the long tube (L/D = 10) is also greater than that through a simple orifice, for a specific driving pressure, although friction in the tube has reduced the outflows from the short-tube values.

The simplest modelling of non-steady flow through these apertures is, of course, the hypothesis that the curves of Figure 2 are accurately traced during each cycle. The results of this investigation can most readily be presented as process paths in the plane C_d vs driving pressure or flow rate.

Figure 3 displays traces representing the three variables measured in the non-steady flow tests. As would be expected, in view of the smooth area variation provided by the interrupter disc in the inlet pipe, the variations of the three quantities are relatively smooth, with the pressure waveform being approximately sinusoidal. Signal noise arises from some disturbances within the flow, mechanical vibration transmitted from the fan and instrumentation electronics.

Figure 4 shows the effect of frequency for the long tube (L/D = 10) on the values of C_d plotted against driving pressure throughout the flow cycle. The driving pressure, p, comprises a mean and harmonic component, viz: $p = p_m + p_o \sin\omega t$. At aperture outlet the pressure is atmospheric, thus the driving pressure is also the pressure difference across the aperture. The ratio of fluctuating pressure component amplitude to mean pressure R_p was held constant at approximately 1, for the tests in Fig. 4. The results for the two lower frequencies (Fig 4 a and b) display an interesting feature, namely, that the values of C_d for high pressure differentials, say, 250 to 350 Pa (C_d = 0.77) are higher than the corresponding steady-flow values for the long-tube case shown in Figure 2 (C_d = 0.75).

As would be expected, the variations of C_d depart more markedly from a uniform value as the frequency of the flow fluctuation increases. However, even at the lowest frequency considered, 0.05 Hz, there are departures from the near-steady-state value. Note that the long-tube steady-state values presented in Figure 2 show no significant variation in the flow range $\dot{V} \geqslant 3$ l/s, corresponding to $p \geqslant 40$ Pa. Hence, the response for low pressure differentials must be attributed to some effect of non-steadiness, either in the flow itself or in the instrumentation system.

Figures 5(a) to (d) show the effect of a progressive increase in the amplitude of the imposed pressure variation (R_p range from 0.16 to 0.93). For

the lowest amplitude (Figure 5(a)) the value of the discharge coefficient remains sensibly constant throughout each cycle, and throughout the three cycles considered. The mean value of C_d is, however, a little higher (0.77 compared with 0.75) than the steady-state value of Figure 2.

The measurements of Figures 5(b) and (c) are less closely bunched for any one cycle and, what is more, display a degree of variability from one cycle to the next. Finally, the results for the highest amplitude, Figure 5(d), are widely spread, although the cycle-to-cycle variation is only moderate.

Figures 6(a) to (c) present variations of the discharge coefficient for closely similar pressure variations imposed across the three aperture geometries. In each case the values of C_d have been normalised by division by a value of C_d representative of steady, high Reynolds-number flow, the values chosen being 0.62 for the orifice, 0.76 for the short tube configuration, and 0.74 for the long tube. As might be expected, the results for the orifice plate and short-tube are rather similar, although the variation in C_d around the cycle is somewhat less for the short-tube. The variation in the discharge coefficient is considerably greater when the long tube is affixed at the exit. This behaviour can be ascribed to the enhanced role of inertia, the considerable column of air in motion within the tube possessing a 'memory' of the pressure differentials pertaining earlier in the cycle. The theoretical analysis which follows develops this idea in a more explicit fashion.

5 THEORY

The model considered is shown in Fig.7. It consists of a large reservoir in which a fluctuating pressure ($p_1(t)$) drives a flow ($\dot{V}(t)$) through an aperture of cross-sectional area A_o. Downstream of the opening the pressure is p_2 and may also fluctuate, although it was held constant in the tests reported here.

The pressure difference/flow relationship for the flow geometries investigated experimentally can be characterised by a discharge coefficient, C_d. This coefficient is defined in the usual way as:-

$$C_d = \frac{\dot{V}}{A_o \left[2(p_1 - p_2)/\rho\right]^{1/2}} \qquad (1)$$

and is taken to apply to both steady and unsteady (based on instantaneous values) flows.

Two cases are considered: a plane aperture (orifice) as shown in Fig.7a and a cylindrical aperture which is assumed long enough for internal flow reattachment to occur (Fig.7b). Whilst there are features in common, the two cases are treated separately, for clarity. In both cases results are derived for instantaneous and averaged discharge coefficients in terms of prescribed single harmonic flow waveforms. The flow path lengths through the apertures are small compared with the flow pulsation wavelengths; accordingly the flow is treated as incompressible.

5.1 (a) Plane Aperture (Orifice, Fig.7a).

The theoretical results for C_d is derived as follows; initially, considering the flow to be inviscid, the equation of motion is:-

$$-\frac{1}{\rho}\frac{\partial p}{\partial z} = \frac{\partial v_z}{\partial t} + v_z\frac{\partial v_z}{\partial z} + v_r\frac{\partial v_z}{\partial r}$$

It is assumed that v_z can be written as $\dot{V}/A$, where A is the local flow cross-section, which is assumed to be time invariant. Integration with respect to z between stations 1 (reservoir) and 2 (vena contracta) yields:-

$$(p_1 - p_2)/\rho = \frac{\ell}{A_o}\frac{d\dot{V}}{dt} + \frac{\dot{V}^2(1+k)}{2(C_c A_o)^2} \qquad -(2)$$

ℓ is defined as $A_o\int_1^2 dz/A$ and the coefficient k is introduced to allow for frictional effects in the flow. C_c is the coefficient of contraction at the vena-contracta. Eliminating p_1-p_2 between equations (1) and (2) produces the result:-

$$C_d^2 = \frac{\dot{V}^2/2A_o^2}{\frac{\ell}{A_o}\frac{d\dot{V}}{dt} + \frac{\dot{V}^2(1+k)}{2(C_c A_o)^2}} \qquad (3)$$

For steady flow this reduces to:

$$C_d^2 = C_c^2\left(\frac{1}{1+k}\right) = C_{ds}^2 \qquad (4)$$

Some insight into the dependence of C_d upon parameters of the flow can be obtained by assuming a periodic flow of the form:-

$$\dot{V} = \bar{\dot{V}} + \dot{V}_o \sin \omega t$$

It should be noted, however, that in our laboratory model tests the applied pressure difference, $p_1 - p_2$, was made to be of sinusoidal form. The flow waveform is prescribed for the theoretical model in order to allow an analytical solution for C_d.

Substitution for $\dot{V}$ into equation (3) then yields:-

$$C_d = \left\{ \frac{1}{\frac{2R St^* \cos\omega t}{(1+R\sin\omega t)^2} + \frac{1}{C_{ds}^2}} \right\}^{1/2} \quad -(5)$$

where $R = \dot{V}_o / \bar{\dot{V}}$. The use of ℓ results in a modified Strouhal number, $St^* = \omega A \ell / \bar{\dot{V}}$. For the experimental study, the ordinary Strouhal number, $St = fD/v$ is used. The two parameters are related as follows: $St^* = St\,\ell/D$.

This result allows the calculation of C_d values throughout a flow cycle. The degree of variation throughout a cycle gives an indication of the errors that would arise from using the steady flow value of the discharge coefficient (C_{ds}), thereby treating the flow as quasi-steady. Forming the ratio C_d/C_{ds} facilitates comparison between apertures of differing geometry, as was shown for the experimental results in Fig.6. The theoretical results are shown in Fig.8 and were obtained by re-arranging equation (5) to give:-

$$\frac{C_d}{C_{ds}} = \left\{ \frac{1}{1 + \frac{2 C_{ds}^2 R.St^* \cos\omega t}{(1 + R\sin\omega t)^2}} \right\}^{1/2} \quad -(6)$$

5.1 (b) Cylindrical Aperture (Fig.7b)

The pressure difference between station 1 and the vena contracta (v) can be written in the same form as equation (2):-

$$(p_1 - p_v)/\rho = \frac{\ell'}{A_2} \frac{d\dot{V}}{dt} + \frac{\dot{V}^2(1+k')}{2(C_c A_2)^2} \quad -(7)$$

The prime added to ℓ and k denotes the different inertial and viscous effects which arise from the presence of a solid boundary between the reservoir and vena-contracta.

Application of the momentum equation to a control-volume encompassing all fluid in the aperture between the full cross section at the vena-contracta and aperture exit yields:-

$$(p_v - p_2)A_2 = \alpha \tau_o \pi D \ell + \rho \dot{V}(v_2 - v_v) + \rho V \beta \frac{dv_2}{dt} \qquad (8)$$

where τ_o is the skin friction produced by fully developed flow and the coefficient α allows for the non-uniformity of the flow field. There is assumed to be no net momentum flux into the control volume from within the separation 'bubble'. Hence entering momentum is given by $\rho \dot{V} v_v$, where $v_v = \dot{V}/C_c A_2$. The last term on the right in equation (8) represents the rate of change of momentum of fluid within the control volume (volume, $V = \pi D^2 \ell$) expressed in terms of the space-average velocity $v_2 = \dot{V}/A_2$. The coefficient β allows for the non-uniform velocity distribution within the control volume.

Re-arranging equation (8) and writing τ_o in terms of a skin friction coefficient C_f ($= \tau_o / \frac{1}{2}\rho v_2^2$) gives:-

$$p_v - p_2 = \frac{\rho \dot{V}^2}{2A_2^2}\left[4\alpha \frac{C_f \ell}{D} + 2\left(1 - \frac{1}{C_c}\right)\right] + \beta \frac{\rho \ell}{A_2}\frac{d\dot{V}}{dt} \qquad (9)$$

Addition of equations (8) and (9) yields an expression for $p_1 - p_2$. Hence, by substitution for $p_1 - p_2$ into equation (1) and putting $A_o = A_2$, the following result is obtained

$$C_d = \left\{ \frac{1}{\frac{1}{C_{ds}^2} + 2(\ell' + \beta\ell)\frac{A_2}{\dot{V}^2}\frac{d\dot{V}}{dt}} \right\}^{1/2} \qquad (10)$$

Again, for the prescribed flow $\dot{V} = \bar{\dot{V}} + \dot{V}_o \sin\omega t$ equation (10) gives

$$\frac{C_d}{C_{ds}} = \left\{ \frac{1}{1 + \frac{2C_{ds}^2 R.St^* \cos\omega t}{(1 + R\sin\omega t)^2}} \right\}^{1/2} \qquad (11)$$

the same result as equation (6) except that the modified Strouhal number is defined by $St^* = \omega A_2 \mathcal{L} / \bar{V}$ and the inertial length is now $\mathcal{L} = \mathcal{L}' + \beta l$.

The steady flow discharge coefficient is now given by

$$C_{ds} = \frac{C_c}{\left[1 + k' + 4\alpha C_c^2 C_f l/D + 2C_c(C_c - 1)\right]^{1/2}} \qquad (12)$$

The middle 2 terms of the denominator in equation (12) represent friction effects, the last term represents pressure recovery due to spatial deceleration of the flow downstream of the vena contracta. The balance between friction effects and pressure recovery depends upon the ratio L/D of the aperture.

5.2 Comparisons Between Theory and Experiment

Theoretical curves of C_d/C_{ds} for the three flow geometries tested are shown in Fig.8. Parameter values used are similar to those for the experimental results presented in Fig.6. The theory shows the same general features as the experimental results, particularly for the case L/D = 10. The predicted 'loop' size for the orifice case was, generally, smaller than that derived from experimental results. For the aperture with L/D = 1, the flat-bottomed characteristic of the loop is not predicted. This is probably related to the tube being insufficiently long for flow reattachment to occur continuously throughout the flow cycle.

A direct comparison between theory and experiment for the L/D = 10 aperture is shown in Fig.9. The 'inertial length', $(\mathcal{L}' + \beta l)/D$, is not a measurable quantity, and whilst a value of about 15 appears to be physically justifiable, it does not provide a very good fit with the experimental results which again produce a larger loop. As expected, higher values of this inertial parameter produce broader loops.

From equations (6) and (11) it is possible to identify, for a given value of the parameter R, the value of RSt* that would give a specified error in C_d relative to C_{ds}. Fig.10 shows the 5% error boundaries for the maximum and minimum C_d values occurring in a flow cycle. The region below and to the left of each boundary would give errors below 5%. The corresponding experimental results, which are also

shown in Fig.10, do not establish any clear pattern. As indicated above, C_d loops from measured data are larger than predicted by theory. Therefore, the experimental results produce more conservatively located error boundaries than those obtained from equations (6) and (11).

5.3 Time-Averaged Discharge Coefficients

In addition to instantaneous values of C_d, time-averaged values may also be defined and determined by integration. For example, $\bar{C}_d$ is defined as in equation (1), but using time-averaged values of both the flow and the square root of the fluctuating driving pressure difference, as follows:-

$$\bar{C}_d = \bar{\dot{V}} / A_o (2/\rho)^{1/2} \overline{(p_1 - p_2)^{1/2}} \qquad (13)$$

Similarly, an rms discharge coefficient $\sqrt{C_{dm}^2}$ can be defined, again using equation (1), but this time based upon time-averaged values of the flow rate squared and the time-averaged pressure difference, as follows:-

$$\sqrt{C_{dm}^2} = \left[\overline{\dot{V}^2} / A_o^2 (2/\rho) \overline{(p_1 - p_2)} \right]^{1/2} \qquad (14)$$

If the flow rate is represented more generally as:-

$$\dot{V} = \bar{\dot{V}} + \dot{V}'(t)$$

then, from the measured fluctuating pressure difference, $p_1 - p_2$, it is possible to calculate the mean flow, $\bar{\dot{V}}$, using $\bar{C}_d$. Also the mean-squared fluctuating flow component may be calculated by using both $\bar{C}_d$ and C_{dm}^2 as follows:-

$$\overline{(\dot{V}')^2} = (2A_o^2/\rho) \left\{ C_{dm}^2 \overline{(p_1 - p_2)} - (\bar{C}_d)^2 \left[\overline{(p_1 - p_2)^{1/2}} \right]^2 \right\}$$

Results for $\bar{C}_d$ and $\sqrt{C_{dm}^2}$ obtained from tests with the plane aperture over the full range of parameter values are shown in Fig.11. The results are normalised with respect to C_{ds}, taking a value appropriate for higher flow rates (= 0.62, see Fig.2). An approximate value of the normalised time-averaged coefficients is 1.02 for both cases.

The somewhat greater scatter for tests at the lower mean pressure (p_m = 28 Pa) is thought to be partly due to a poorer signal to noise ratio at lower flows. Also the steady flow behaviour of C_d is more variable at low flow rates and generally exceeds the value of 0.62 (Fig.2).

As might be expected for coefficients derived from integrated results, there is a much weaker dependence on the unsteadiness parameters than is the case for the instantaneous C_d data. Departures from the nominally constant values of $\overline{C}_d$ and $\sqrt{C_{dm}^2}$ begin to occur at R.St = 0.006.

6 DISCUSSION

6.1 Effects of Finite Volume of Plenum Chamber

A plenum chamber of finite volume is desirable in order to produce a disturbance free flow-source upstream of the aperture (Fig.1). In order to obtain the inflow waveform, measurements are made with an anemometer located in the tube supplying the plenum. A disadvantage of this arrangement is the facility for transient mass storage within the plenum due to the compressibility of air. This effect produces a flow cycle through the aperture which differs from that measured in the supply tube. Treating the process as an isentropic compression (or expansion) of an ideal gas yields the result for transient mass storage

$$\frac{dm}{dt} = \frac{V}{R_g T}\frac{dp}{dt}$$

Variations in dm/dt depend upon dp/dt, since $V/R_g T$ is sensibly constant. In the laboratory model, the driving pressure difference is given approximately by $p = p_m + p_o \sin \omega t$ so, clearly, dp/dt is greater at higher frequencies and amplitudes.

The effect of this transient storage was examined in one test in which the plenum pressure signal was subjected to analogue differentiation and then recorded in parallel with the other instrumentation signals. The corrected volume flow rate through the aperture, $\dot{V}_2$, is then given in terms of the measured flow rate in the inflow tube, $\dot{V}_1$, by:

$$\dot{V}_2 = \dot{V}_1 - \frac{V}{\gamma p}\frac{dp}{dt}$$

C_d values based upon the measured and then upon the corrected flow rates are shown in Fig.12. This test was at a relatively high frequency (0.6Hz) and large amplitude ($R_p = p_o/p_m = 0.96$) and, as a result, the corrected flow produces a larger C_d loop than from the measured flow.

6.2 Comment on unsteadiness effects

A somewhat surprising result from the experimental study is the apparently detectable effect of unsteadiness upon C_d at relatively low frequencies (e.g. f = 0.05 Hz and St = 10^{-4}) as shown in Fig. 4a. The question arises of the adequacy of instrumentation frequency response. The pressure transducer has a resonant frequency of several kHz in air, but the velocity transducer has a time constant of about 0.1s.

Further tests are in progress to determine if there is a time-lag introduced in the infered instantaneous flow signal which may distort the C_d result. Corrections for compressibility effects within the plenum tend to increase the area of the C_d loops (Fig. 12).

7 CONCLUSIONS

1. Pulsatile (but non-reversing) flows through a range of aperture geometries have been investigated.

2. The relationship between instantaneous pressure-difference and flow has been characterised by a discharge coefficient, C_d. Hence, for a given flow cycle a C_d "loop" is formed; the width of the loop depends upon the relative importance of inertial effects in the flow.

3. Discharge coefficients based on time-averaged quantities have been defined and measured.

8 REFERENCES

Earles, S.W. and Zarek, J.M. (1963), "Use of sharp-edged orifices for metering pulsating flow" I.Mech.E.Proc. 177, 997-1012.

Karim G.A. and Rashidi M. (1972) "The measurement of a pulsating air flow using a sharp-edged orifice meter" ASME J. Fluid Engineering 94, 1-8.

Mohammad, W.A. and Mottram R.C. (1981) "High frequency pulsation effects on orifice meter accuracy" in Advances in Flow Measurement Techniques, BHRA Warwick, 81-94.

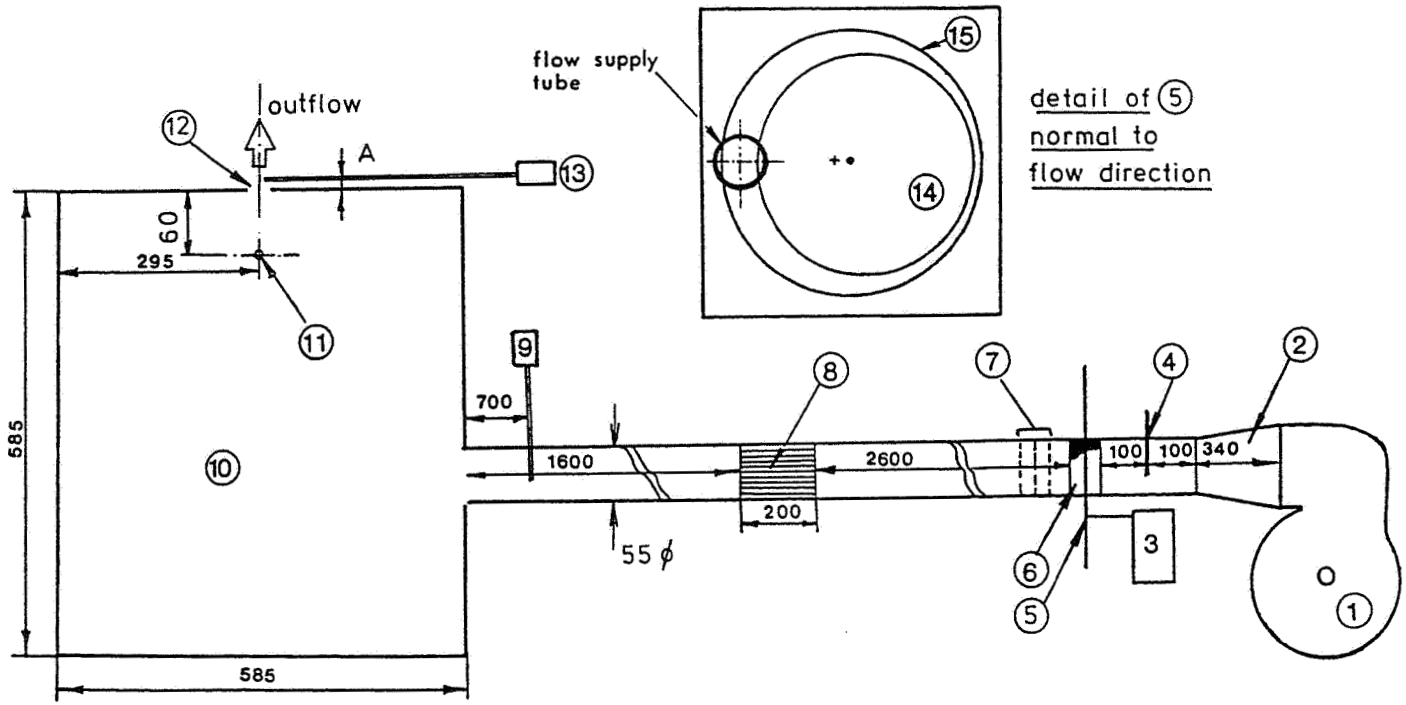

Figure1 : Dimensions in mm; not to scale

1. AEI 2 h. p. centrifugal fan drawing in room air
2. Matching section between fan outlet and duct
3. Motor with reduction gears to drive disc (14)
4. Mean flow control damper
5. Fluctuation-inducing mechanism (see inset)
6. Brush seal for rotating disc
7. Smoothing screens
8. Flow straightener
9. TSI anemometer
10. Plenum chamber (depth 590 mm into plane of figure)
11. Wall pressure tapping
12. Orifice or other aperture
13. TSI anemometer
14. Rotating disc, diameter 273 mm
15. Circular hole surrounding disc, diameter 320 mm

A. Dimension defining position of second anemometer probe (either one diameter from plane of orifice or 10 mm from end of a tube).

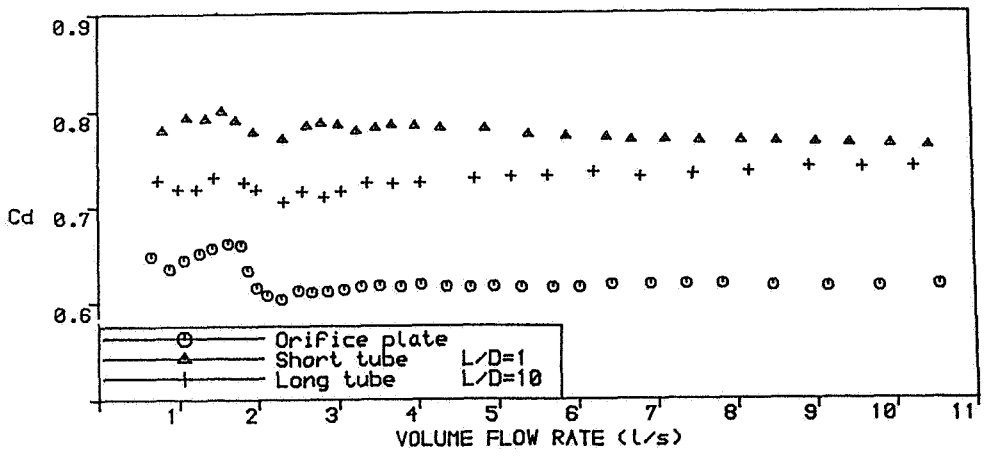

Figure 2. Steady flow results — discharge coefficient

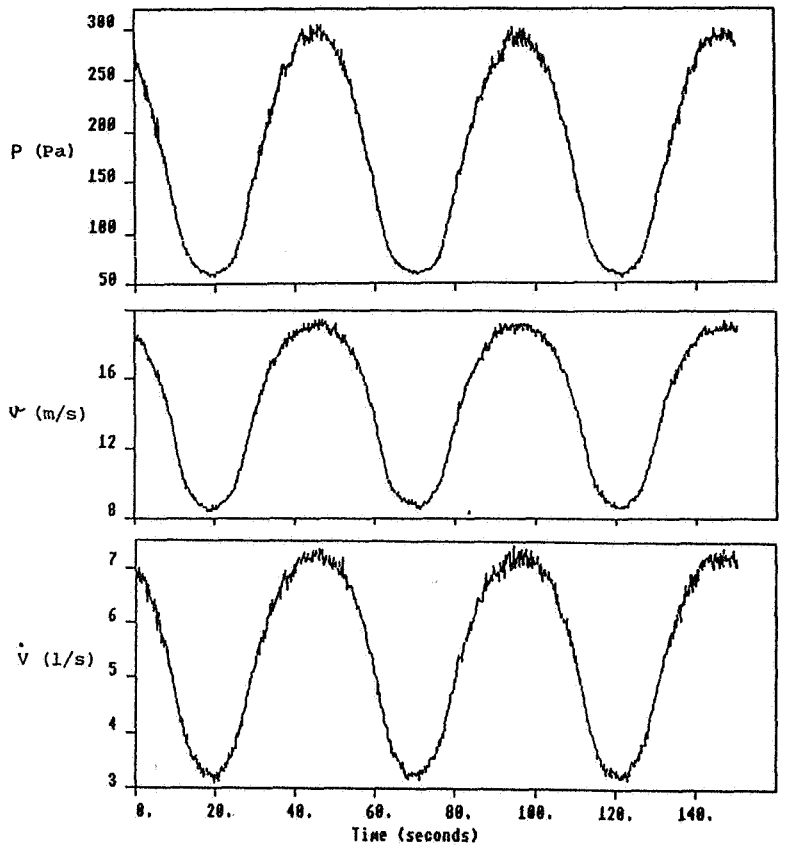

Figure 3 Raw data (in descending order: pressure difference, velocity and volume flow rate) for test with the following conditions: f = 0.02 Hz, p_m = 178 Pa, $\hat{V}$ = 5.42 ℓ/s and R_p = 0.72.

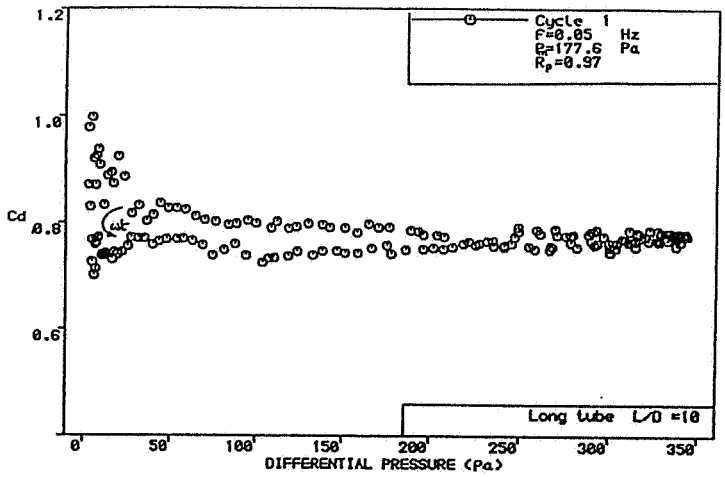

(a)

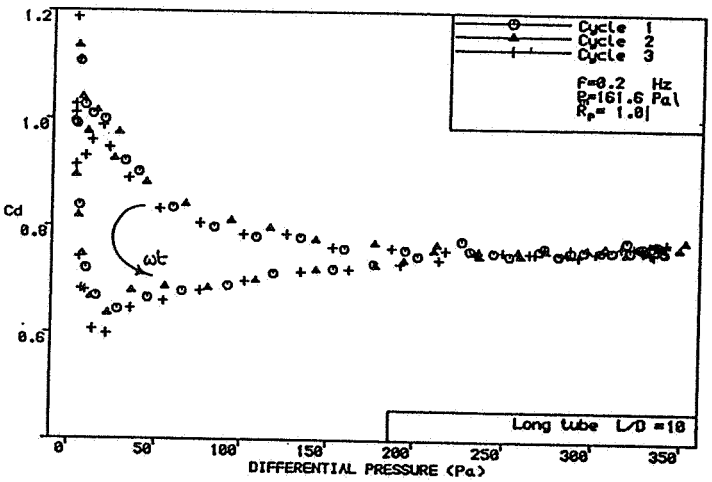

(b)

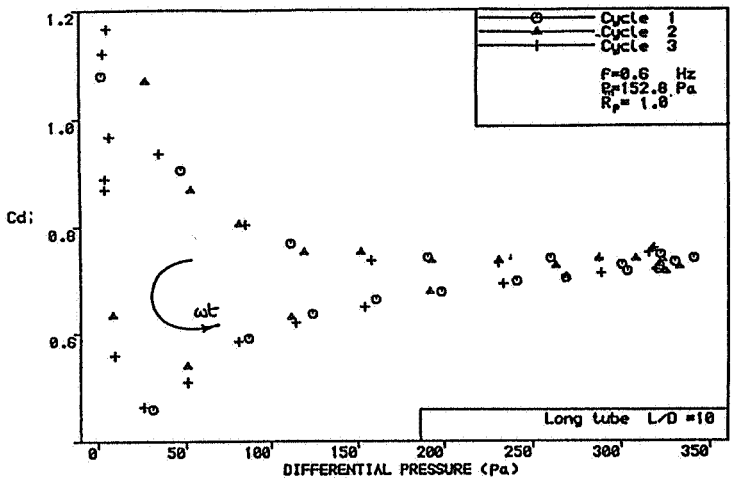

(c)

Figure 4. C_d values for the long tube plotted against driving pressure difference to show variations throughout the flow cycle for progressively increasing frequency (a) f = 0.05 Hz, (b) f = 0.2 Hz, and (c) f = 0.6 Hz.

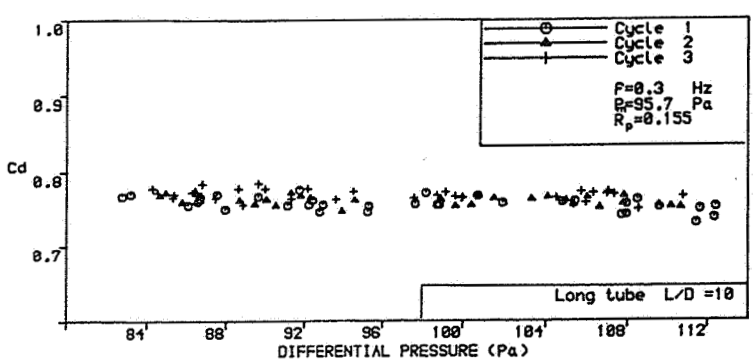

(a)

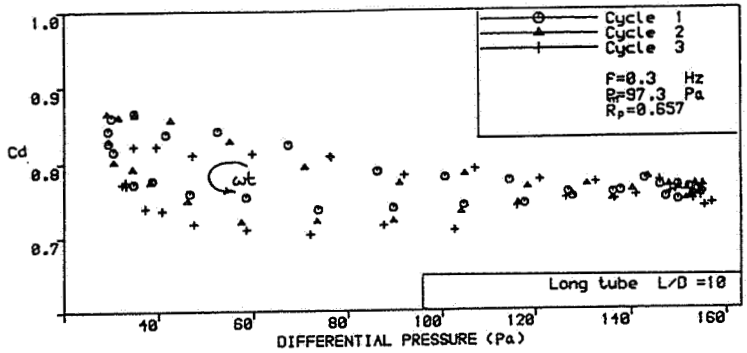

(c)

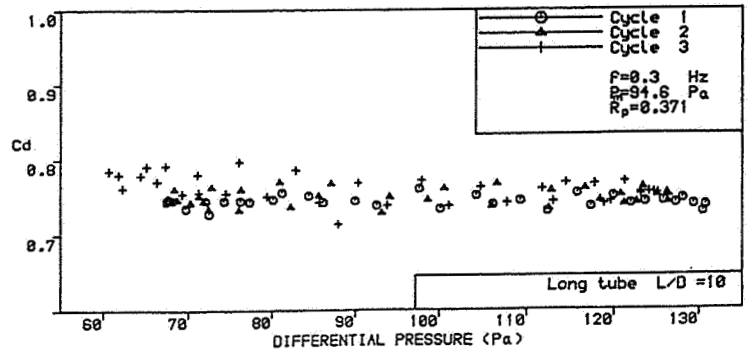

(b)

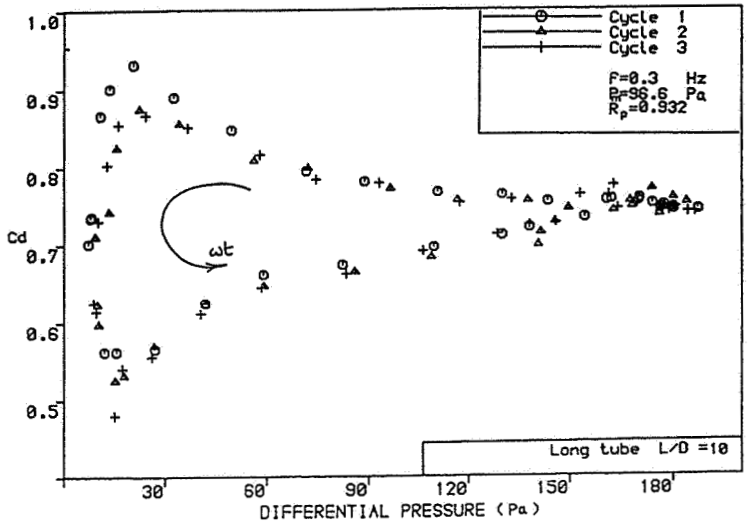

(d)

Figure 5. C_d values for the long tube plotted against driving pressure difference to show variations throughout the flow cycle for progressively increasing amplitude (a) R_p = 0.155, (b) R_p = 0.371, (c) R_p = 0.657, (d) R_p = 0.932.

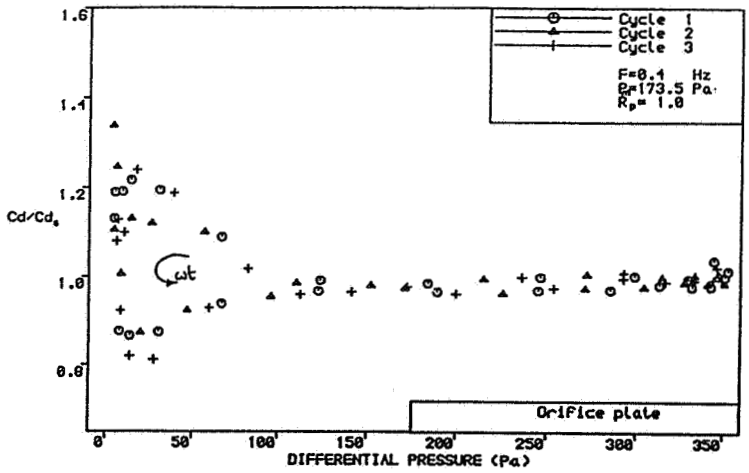

(a)

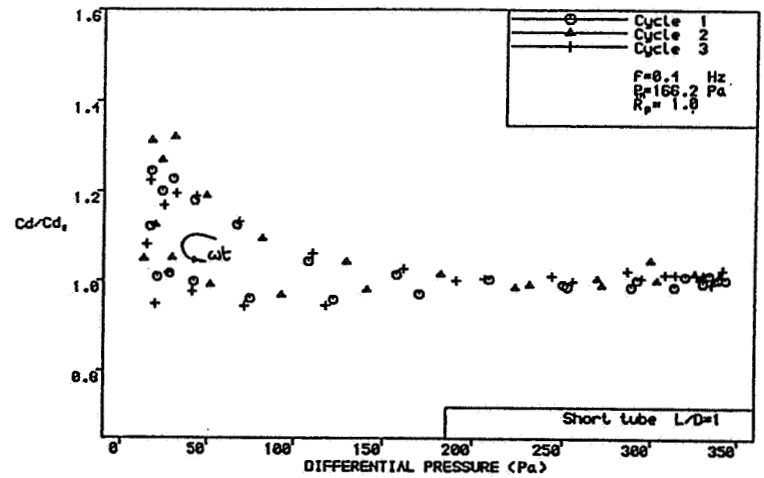

(b)

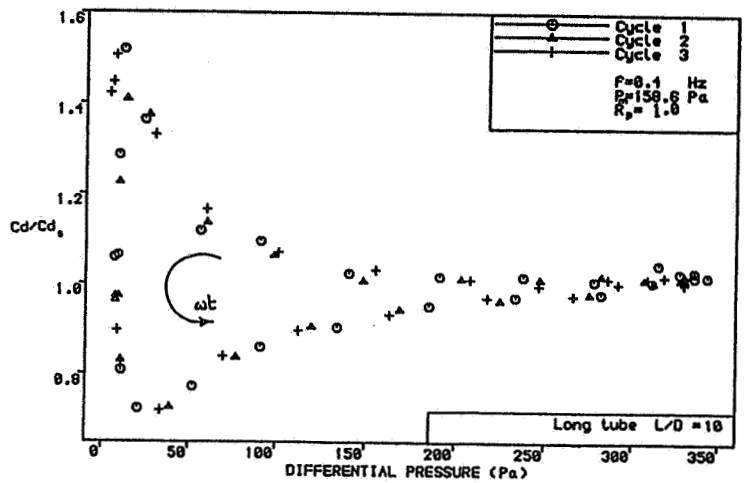

(c)

Figure 6 C_d values showing variations throughout the flow cycle with nominally constant operating conditions for (a) orifice, (b) short tube and (c) long tube.

Figure 7 Geometry for aperture theoretical models (a) orifice (b) tube.

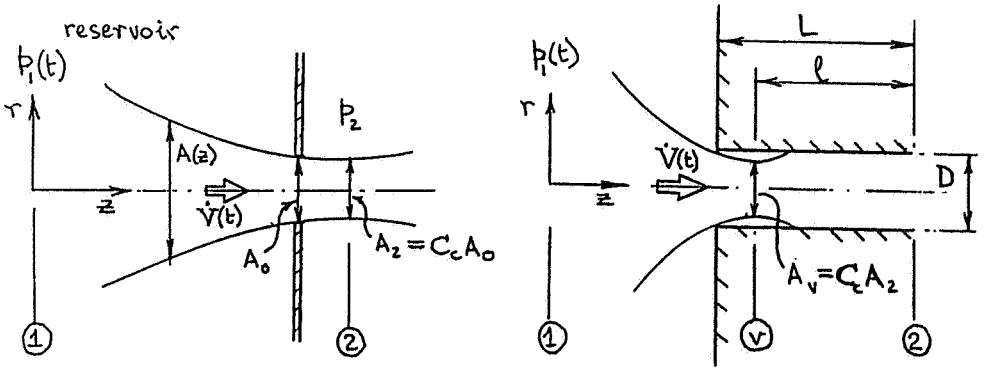

Figure 8 Theoretical results for C_d.

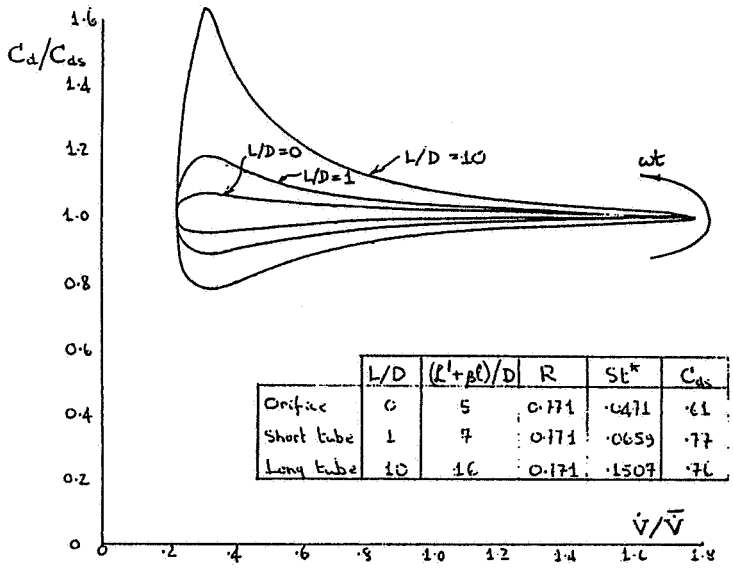

	L/D	$(\ell'+\beta\ell)/D$	R	St^*	C_{ds}
Orifice	0	5	0·171	·0471	·61
Short tube	1	7	0·171	·0659	·77
Long tube	10	16	0·171	·1509	·76

Figure 9 Comparision between theoretical and experimental results for C_d.

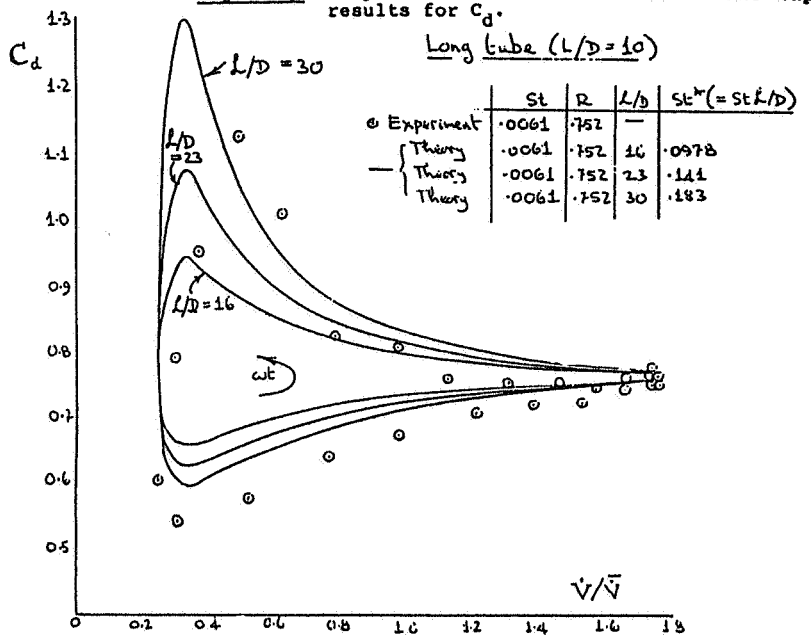

Long tube (L/D = 10)

	St	R	L/D	$St^*(=St\,L/D)$
⊙ Experiment	·0061	·752	—	
— Theory	·0061	·752	16	·0978
— Theory	·0061	·752	23	·141
— Theory	·0061	·752	30	·183

Figure 10 Comparision between theory and experiment for 5% error boundaries for maximum ($\hat{C}_d$) and minimum ($\check{C}_d$) values of C_d.

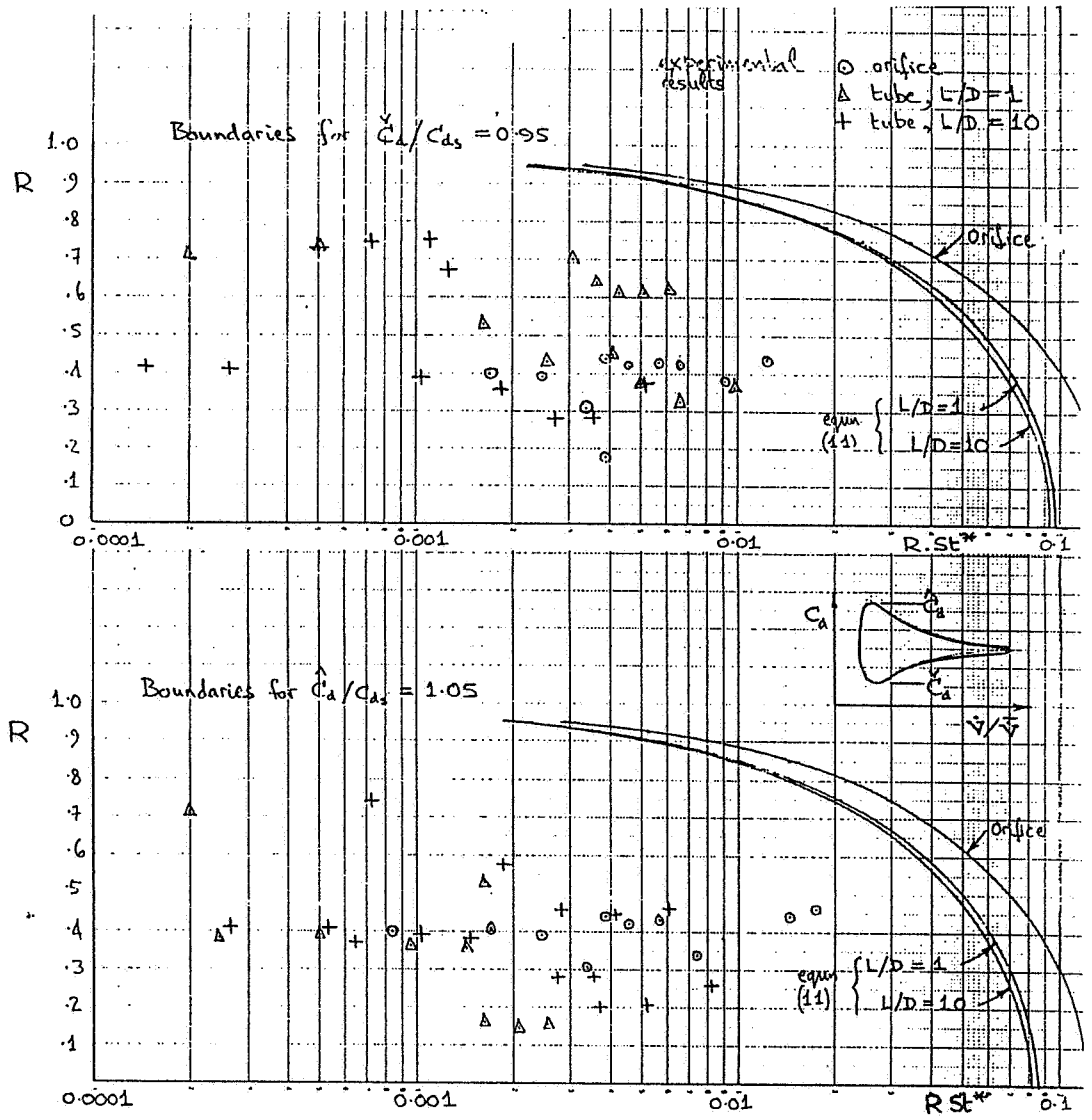

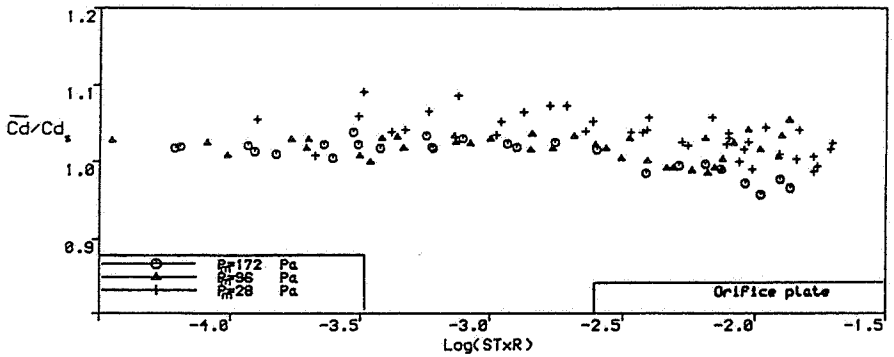

(a)

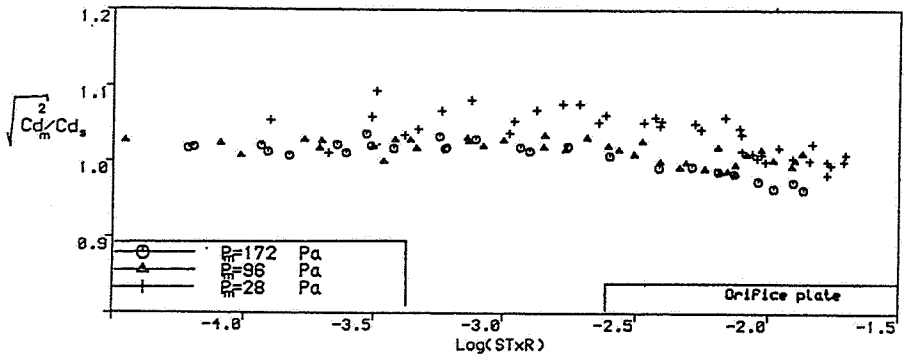

(b)

Figure 11 Experimental results for (a) $\overline{C}_d$ and (b) $\sqrt{C_d^2}_m$.

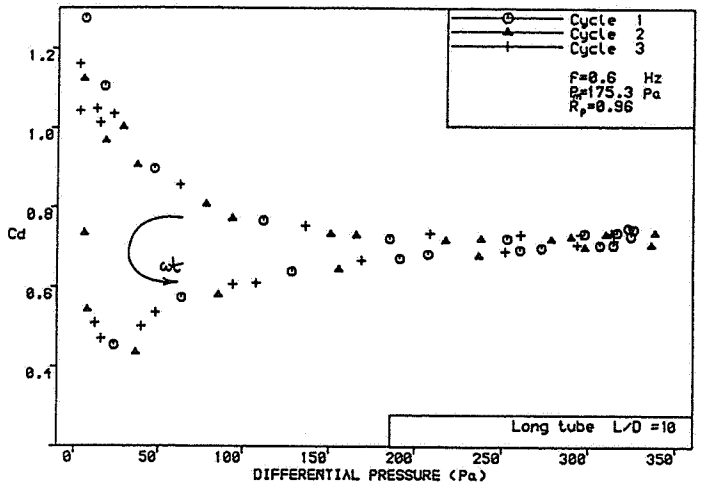

(a)

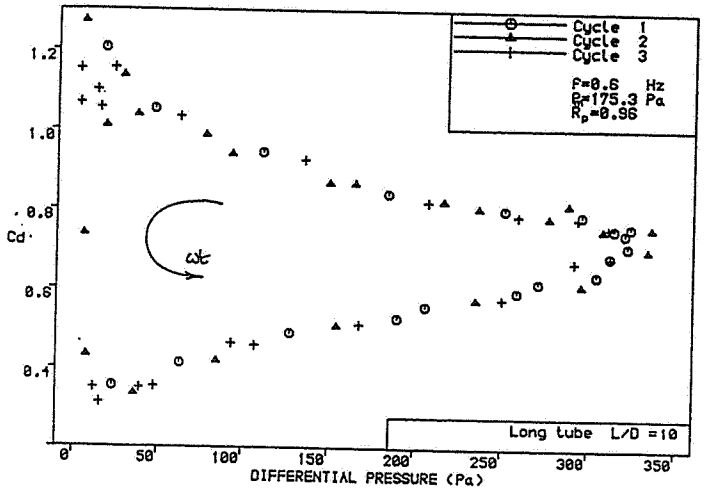

(b)

Figure 12. Effects of changing gas density upon C_d values (a) uncorrected and (b) corrected.

Discussion

Paper 6

M. Bassett (BRANZ) This analysis could have application to airflows through rainscreen claddings. Here it is desirable to know airflow rates through ventilation openings at a range of wind pressure frequencies. Has this been undertaken or contemplated?

B. Sahin (Brunel University, UK) Thankyou for your question - no, we have not considered the application of this work to rainscreen cladding. I would be grateful if you could advise where we can obtain details of the geometry of this cladding and hence, any possible applications of the work.